Short Ballistic Josephson Coupling in Planar Graphene Junctions with Inhomogeneous Carrier Doping

Jinho Park,[1] Jae Hyeong Lee,[1] Gil-Ho Lee,[1] Yositake Takane,[2] Ken-Ichiro Imura,[2]
Takashi Taniguchi,[3] Kenji Watanabe,[3] and Hu-Jong Lee[1,*]

[1]*Department of Physics, Pohang University of Science and Technology, Pohang 37673, Korea*
[2]*Department of Quantum Matter, AdSM, Hiroshima University, Higashi-Hiroshima 739-8530, Japan*
[3]*National Institute for Materials Science, Tsukuba 305-0044, Japan*

We report on short ballistic (SB) Josephson coupling in junctions embedded in a planar heterostructure of graphene. Ballistic Josephson coupling is confirmed by the Fabry-Perot-type interference of the junction critical current I_c. The product of I_c and the normal-state junction resistance R_N, normalized by the zero-temperature gap energy Δ_0 of the superconducting electrodes, turns out to be exceptionally large close to 2, an indication of strong Josephson coupling in the SB junction limit. However, I_c shows a temperature dependence that is inconsistent with the conventional short-junction-like behavior based on the standard Kulik-Omel'yanchuk prediction. We argue that this feature stems from the effects of inhomogeneous carrier doping in graphene near the superconducting contacts, although the junction is in fact in the short-junction limit.

Graphene shows a characteristic linear dispersion (a synthetic relativistic world) in momentum space, whereas its real-space nature is also very unique, realizing a hitherto unknown perfectly two-dimensional world [1–3]. The exotic proximity properties arising from this intrinsic linear dispersion in graphene have been studied with the graphene-superconductor heterostructures [4–8]. In particular, a planar graphene Josephson junction (pGJJ), formed by arranging two superconducting electrodes in close proximity on a graphene layer, have been widely adopted [7–12]. While these studies of pGJJs took good account of the linear dispersion, the unusual characteristics of pGJJs reflecting the unique planar nature of graphene have not been fully paid attention to.

In a pGJJ the superconducting order of the two adjacent superconductors is coupled by forming the Andreev bound state in the graphene insert. In the ballistic limit ($L < l_{\mathrm{mfp}}$; l_{mfp} = mean free path), the Josephson current flows via well-defined Andreev bound state channels. In the limit of a short junction ($L < \xi$; L = junction channel length, ξ = superconducting coherence length), the coherence of the Josephson coupling becomes more robust than in a long junction ($L > \xi$), with the coupling being mediated via a single Andreev bound state without mixing of quantum states among different channels. Thus, short ballistic (SB) strong Josephson coupling is essential to realizing coherent quantum states such as Andreev-level qubits [13,14]. In addition, as a pGJJ allows gate tuning of the Josephson coupling strength, realizing SB strong Josephson coupling in pGJJs would offer their versatility to quantum device applications.

The SB Josephson coupling has been realized in vertical graphene JJs [15,16], where the channel length is essentially governed by the atomic thickness of the graphene insert. Ballistic JJ characteristics have recently been realized in pGJJs prepared by hexagonal-boron-nitride (hBN) encapsulation of a graphene layer together with atomic edge contacts of superconducting leads [17–21]. However, the short junction characteristics are not yet fully confirmed in the ballistic limit. An earlier report claiming the SB Josephson coupling in a pGJJ [18] exhibited a too low $I_c R_N$ product (I_c, junction critical current; R_N, normal-state junction resistance) and an exponential decay of $I_c(T)$ for increasing temperature near T_c (see Fig. S5), a canonical long-junction behavior by conventional wisdom [22]. Furthermore, these previous studies lack the quantitative explanation on the effective carrier transmission near graphene-superconductor interfaces in a pGJJ arising from the work-function difference between graphene and superconducting layers.

Here, we report on the SB Josephson coupling in pGJJs with an Al superconducting contact. With a relatively small superconducting gap, Al provides a long superconducting coherence, which is advantageous for realizing a short junction ($L < \xi$). The value of $I_c R_N$ of pGJJs normalized by Δ_0/e in this study (~2.0) is much larger than the ones obtained previously in a pGJJ [18], in which SB characteristics were claimed. The normalized value is close to the theoretically predicted one (~2.4) for an ideal SB proximity graphene JJ [23]. Especially, we focused on the T dependence of I_c to examine the SB nature of our pGJJs. For the $I_c(T)$ fit, we adopted the theoretical model [24,25] taking
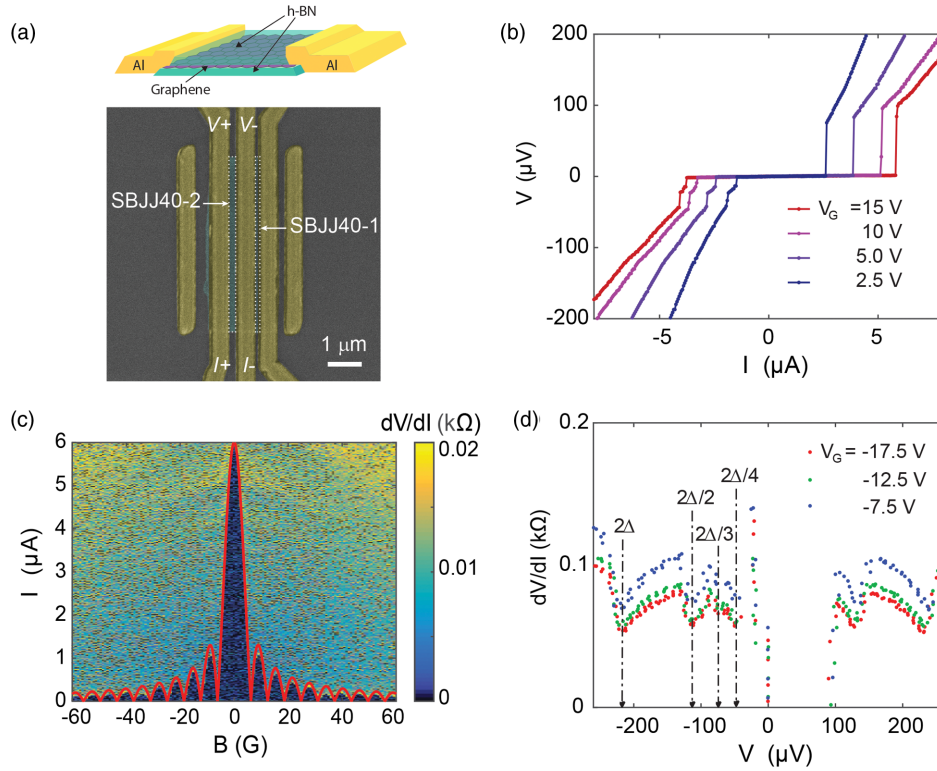
FIG. 1. (a) (Upper panel) Schematic diagram of our planar graphene Josephson junctions (pGJJs) with boron nitride (BN)-encapsulated graphene contacted by Al electrodes. (Lower panel) False-colored scanning electron microscopy (SEM) image of two pGJJs: SBJJ40-1 (channel length: ∼120 nm) and SBJJ40-2 (channel length: ∼220 nm). (b) Current-voltage characteristic curves of SBJJ40-2 for different gate voltages V_G. Bias current was swept from negative to positive. (c) Differential resistance map as a function of magnetic field and bias current: the Fraunhofer pattern. (d) Bias spectroscopy with dips in the differential resistance of the junction arising from multiple Andreev reflection.

into account carrier doping near the graphene-superconductor interfaces. The two-dimensional nature of graphene significantly enhances the doping effect on $I_c(T)$ of a junction. $I_c(T)$ curves of our pGJJs show a near-perfect fit with this model, whereas they are in apparent discord with the conventional Kulik-Omel'yanchuk (KO) prediction [26–28], which is often used to examine the coupling characteristics of a proximity JJ. This study provides a quantitative investigation on the SB pair coupling modified by inhomogeneous doping near the graphene-superconductor interfaces.

We prepared a stacked hexagonal boron nitride (hBN)-graphene-hBN structure using a dry-transfer technique [29]. Superconducting contacts to the monolayer graphene were made at the junction edges, exposed by the O_2/CF_4 plasma etching of BN flakes and the graphene layer simultaneously. Edge contacts were made to the graphene layer [29] by *in situ* electron-beam deposition of two Al/Ti bilayer (60/6 nm thick) superconducting electrodes. Two junctions were prepared simultaneously: SBJJ40-1 and SBJJ40-2 [right and left in Fig. 1(a)]. The physical scale of the junctions was estimated by scanning electron microscopy; both had a common channel width of ∼4.7 μm, and channel lengths of ∼120 nm (SBJJ40-1) and ∼220 nm

(SBJJ40-2). The junction resistance was measured by a quasi-four-probe scheme, in which the contact resistance (R_c) of two graphene-Al interfaces was included [see Fig. 1(a)].

All of the data in this Letter, except for the T dependence, were taken at the base temperature of 15 mK. Figure 1(b) shows typical Josephson behavior of the current-voltage curves for SBJJ40-2, with sharp switching to the resistive state at different values of I_c for varying gate voltages (V_G). The large hysteresis in the current-voltage curves is believed to arise mainly from self-heating [30]. The regular magnetic-field modulation of I_c [Fraunhofer pattern; Fig. 1(c)], satisfying the relation $I_c = I_0|(\sin \pi\Phi/\Phi_0)/(\pi\Phi/\Phi_0)|$, corresponds to a uniform current distribution along the width of the junction. Here, I_0 is the critical current in zero field, Φ is the perpendicular magnetic flux threading the junction area, and Φ_0 is the flux quantum. The B-field period of the oscillation ∼6.2 G yields $L + 2\lambda \sim 710$ nm, where the field penetration depth λ (∼250 nm) is in good accord with previous reports [31,32]. Figure 1(d) shows the measured differential resistance as a function of the bias current; clear dips appeared via multiple Andreev reflections, leading to an estimation of Δ_0 (∼110 μeV) by matching the dip positions with $2\Delta_0/n$ for the best-fit integer values of n.
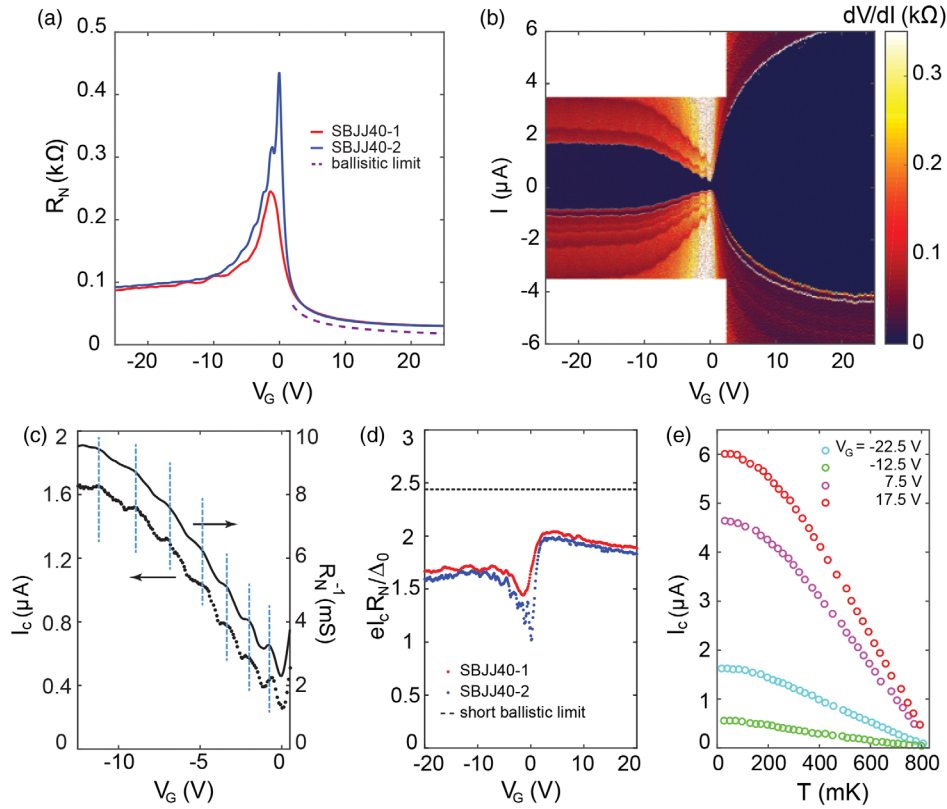
FIG. 2. (a) Normal-state junction resistance R_N of SBJJ40-1 and SBJJ40-2 measured at 4.2 K for varying V_G. The dashed line corresponds to the ballistic limit with perfect transmission ($\tau = 1$). (b) Differential resistance map of SBJJ40-2 as a function of I and V_G. (c) In-phase Fabry-Perot oscillation of the junction critical current I_c and the normal-state conductance $(R_N)^{-1}$ of SBJJ40-2, which indicates ballistic pair transport. The vertical guide lines show the in-phase oscillation between the two curves. (d) The $I_c R_N$ product normalized by Δ_0/e of SBJJ40-1 and SBJJ40-2 for varying V_G. The dotted line is the theoretical limit, ~ 2.4, for a short ballistic (SB) pGJJ. (e) $I_c(T)$ of SBJJ40-2 for various V_G.

Figure 2(a) shows R_N measured at 4.2 K for varying V_G. The asymmetry of the resistance between negative and positive sides of V_G is due to electron doping of the graphene layer near the electrode contact induced by the Fermi level mismatch. This leads to a junction resistance at positive V_G that is significantly lower than that of the negative side, where a less transmitting n-p-n junction forms. The Fabry-Perot oscillation observed at negative V_G, due to the interference of reflected carriers at the two p-n boundaries, indicates the ballistic transport in the graphene insert. Comparing R_N at positive V_G with the ballistic-limit value of $R_Q = (h/4e^2)(1/N)$ leads to a contact resistivity of ~ 30 $\Omega\mu$m, which corresponds to a total transmission probability of $\tau = R_Q/R_N > 0.70$ for $V_G > \sim 2$ V. Here, $N[= (2W/\lambda_F)]$ is the number of carrier propagation modes for the channel width W and the Fermi wavelength λ_F. Figure 2(b) shows the dV/dI map of SBJJ40-2 as a function of the bias and V_G, where the boundary of the dark blue region represents $I_c(V_G)$ of the junction. $I_c(V_G)$ also exhibited asymmetry across the Dirac point, similar to the one in $(R_N)^{-1}$. I_c exceeded ~ 6 μA at the highly transmitting n-doped region, whereas it was reduced to ~ 1 μA at the p-doped region. We emphasize

that I_c in our device is comparable to those of previous reports on pGJJs of similar widths [17,18]. However, as the junctions consisted of Nb [17] and MoRe [18] superconducting electrodes with gap sizes larger than Al by an order, the normalized coupling strength of our junctions is significantly higher than in those previous reports.

We confirmed the ballistic nature of the Josephson coupling by the oscillation of I_c with V_G, which is in phase with the oscillation of $(R_N)^{-1}$ due to the Fabry-Perot interference [Fig. 2(c)]. This provides direct evidence for ballistic Josephson coupling [33–35] in our devices, which is mediated by the coherent transport of ballistic quasiparticles via the Andreev bound channel in graphene. Similar ballistic pair transport has been reported in pGJJs [17–20]. The coherence length in our pGJJs was estimated to be $\xi = \hbar v_F/2\Delta_0 \sim 2.3$ μm, where $\hbar$ is the Planck's constant divided by 2π and v_F is the Fermi velocity in graphene. Based on the channel lengths of our junctions (~ 120 nm for SBJJ40-1 and ~ 220 nm for SBJJ40-2), which are much shorter than the estimated value of ξ, our junction should be in the short-junction regime.

Figure 2(d) shows the $I_c R_N$ product (normalized by Δ_0/e) vs V_G for the two pGJJs, the values of which
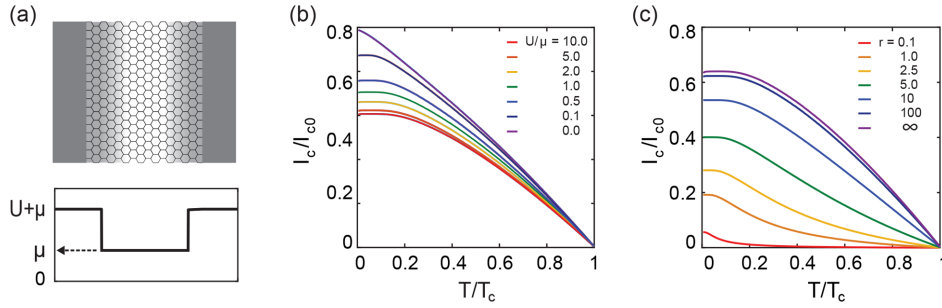
FIG. 3. (a) (upper) Schematic diagram of the spatial distribution of the electrochemical potential in a pGJJ and (lower) the simplified electrochemical potential distribution used in the calculation. The arrow indicates the undoped electrochemical potential in graphene. (b) U/μ dependence of $I_c(T)$ for $r = 100$. (c) $I_c(T)$ for different values of r between 0.1 and infinity for $U/\mu = 5$, which corresponds to $V_G \sim 10$ V in our experiment.

differed by only ~5% under sufficiently doped conditions, although L of the two junctions differed by a factor of 2. The insensitivity of the $I_c R_N$ product to L strongly indicates that our junctions were in the short-junction regime; had they been in the long-junction limit, the shorter junction (SBJJ40-1) would have had a value of $eI_c R_N/\Delta_0$, twofold larger than that of the longer one (SBJJ40-2), as the $I_c R_N$ product for a long ballistic junction is inversely proportional to L. In addition, the $eI_c R_N/\Delta_0$ value itself, reaching up to ~2 in our devices, is close to the theoretical prediction (~2.4) for the SB Josephson coupling in pGJJs [23]. It is an order of magnitude larger than the previous report claiming for the SB Josephson coupling in pGJJs [18] and twice as large as that of a diffusive pGJJ with Al electrodes [9]. This value corresponds to the strongest Josephson coupling among the planar proximity JJs studied to date, including JJs based not only on graphene (~1.0) [9] but also on other insert materials such as semiconducting nanowires (~1.1) [36] and the two-dimensional electron gas system (~0.9) [37].

We examined the junction characteristics based on the T dependence of I_c. $I_c(T)$ curves of SBJJ40-2 for positive V_G (7.5 and 17.5 V) in Fig. 2(e) are monotonically convex upward $(d^2 I_c/dT^2 < 0)$. However, the trend becomes marginal for $V_G = -12.5$ V and even slightly convex downward $(d^2 I_c/dT^2 > 0)$ near T_c for $V_G = -22.5$ V. According to the KO theory, $I_c(T)$ becomes monotonically convex upward only for a short junction for temperatures below T_c. $I_c(T)$ for a long junction should show an exponentially decaying tail near T_c ($\approx 860 \pm 20$ mK for SBJJ40-1 and SBJJ40-2), corresponding to a clearly convex downward behavior, which is qualitatively different from the one for $V_G = -22.5$ V.

Conventionally, the KO theory is used to examine short Josephson coupling characteristics in a proximity JJ. The KO theory, which is valid for a point junction, however, cannot accurately describe the behavior of a wide junction, as used in this study. It is also required to take account of the carrier doping occurring near the graphene-superconductor contact. Thus, we adopt the theoretical

model by Takane and Imura (TI model) proposed recently for SB pGJJs [24,25]. This model includes the effect of both the induced carrier inhomogeneity in graphene and the transparency of the graphene-superconductor interfaces on an equal footing, where $I_c(T)$ may become convex downward even for a pGJJ in the SB regime.

Because of the electronic carrier doping near the graphene-superconductor contact, an electron experiences a potential well and is refracted at the interface. This feature is included in the TI model by adopting the simplified electrochemical potential shown in the lower panel of Fig. 3(a), where μ is the undoped value in graphene and U is its variation due to the carrier doping. The transmission of paired carriers within the graphene layer is determined by U/μ, which also affects $I_c(T)$ of a pGJJ in the SB regime. Another feature of this model is that the tunneling of paired carriers between a graphene sheet and superconducting electrodes is explicitly characterized by using the normalized coupling strength r, which in turn characterizes the interfacial transparency. Thus, the Josephson current and its critical value I_c in the SB regime, which are obtained by applying a quasiclassical thermal Green's function approach to the TI model (refer to the Supplemental Material [38] and Ref. [25] for details), are governed by both U/μ and r. An $I_c(T)$ curve in this model converges to perfect transmission in the KO model as $U/\mu \to 0$ and $r \to \infty$.

Figure 3(b) shows a set of $I_c(T)$ curves, in the SB regime of the TI model, for different values of U/μ in the range between 0 and 10, for the coupling strength r fixed at 100. The overall shape of the curves were relatively insensitive to the variation of U/μ, although $I_c(T = 0)$ continued to decrease with increasing U/μ. However, varying r for a fixed U/μ at 5 resulted in steep changes in the shape of $I_c(T)$, along with a reduction of $I_c(T = 0)$ [Fig. 3(c)]. For $r < 10$, $I_c(T)$ became convex downward approaching T_c from below, whereas it was monotonically convex upward for $r > 10$. The curves become almost insensitive to r for $r > 100$ (see Fig. S2 in Ref. [38]).
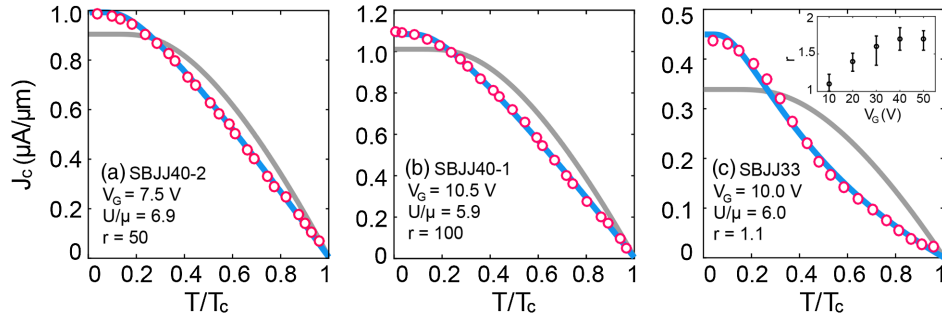
FIG. 4. $I_c(T)$ for three pGJJs; SBJJ40-2, SBJJ40-1, and SBJJ33. Void circles represent data. Fits with the Takane-Imura (TI) and Kulik-Omel'yanchuk (KO) models are shown in blue and gray, respectively. Here, the KO curves are generated for the transmission probabilities of 0.75, 0.72, and 0.64 for the three devices, respectively.

Figures 4(a) and 4(b) show the representative fitting of $I_c(T)$ for SBJJ40-2 (at $V_G = 7.5$ V) and SBJJ40-1 (at $V_G = 10.5$ V) with both the TI and KO models. Both data sets showed convex-upward T dependences, which seem to fit with the regular SB JJ behavior of the KO model. However, the detailed T dependence deviated significantly from the KO prediction. Here, the KO curves were generated for the transmission probability of 0.75 (SBJJ40-1) and 0.72 (SBJJ40-2), the values estimated from the R_Q/R_N ratio of the two junctions [see Fig. 2(a)]. On the other hand, the data sets were well fit by the TI model. In the fitting, r was taken as the best-fit parameter, where U ($=0.6$ eV) was set to be a constant, the work function difference of graphene and titanium, and μ was calculated for a given V_G. The fit led to $r \sim 100$ (notably, the fitting is insensitive to r larger than this value), implying a strong coupling between the Al electrode and graphene layer.

We adopted another pGJJ (SBJJ33), which had a channel length ~ 200 nm similar to SBJJ40-2 (~ 220 nm), again far shorter than ξ. The junction also showed the ballisticity with the Fabry-Perot oscillation both in $(R_N)^{-1}$ and I_c (see Fig. S4 [38]), whereas $eI_cR_N/\Delta_0 \sim 1.0$, which is half the value of SBJJ40-2 yet comparable to or larger than the values of any pGJJs reported previously. $I_c(T)$ curves of this junction changed from convex upward near $T = 0$ to convex downward with increasing temperature near T_c (≈ 680 mK for SBJJ33) [Fig. 4(c)], which is similar to the behavior reported earlier in Ref. [18] (see also Fig. S5 in the Supplemental Material [38]). This does not fit with the conventional theory, either for a short junction with monotonically convex upward $I_c(T)$ or for a long junction with an exponentially decaying tail near T_c, although it is obvious that SBJJ33 was in a short-junction limit as Δ_0 (~ 115 μeV) was much smaller than the Thouless energy E_{th} (~ 2.6 meV). In striking contrast to the conventional KO theory, however, the curves show a near-perfect fit with the TI model over the entire temperature range below T_c with a relatively low coupling strength of $r \sim 1.1$. The high-quality fits were obtained for all the $I_c(T)$ data sets for different gate voltages (Fig. S5 [38]), which implies the relevance of our assumption on the value of $U = 0.6$ eV,

which led to $U/\mu = 6.0$, 4.2, 3.5, and 2.7 for $V_G = 10$, 20, 30, and 50 V, respectively. The value of r increases slightly with V_G [inset of Fig. 4(c)], whereas there is no explicit gate voltage dependence of r in the TI model. It could be accounted for by the fact that the disorder effect from the charged puddles in graphene reduces as V_G increases.

$I_c(T)$ curves of all our pGJJs fit extremely well with the SB behavior of the TI model in the entire temperature range below T_c. While the KO model is valid for a one-dimensional point-contact JJ, pGJJs have an additional momentum degree of freedom in the direction perpendicular to the Josephson current. The spatial carrier inhomogeneity near the superconducting contacts activates this additional degree of freedom, which not only reduces I_c but also modifies its temperature dependence from the KO prediction. Although our junctions consisted of identical contact material in a fully ballistic regime, the junction transmission probability τ differed by $\sim 15\%$ between SBJJ40's and SBJJ33 devices, whereas the two junctions, SBJJ40-1 and SBJJ40-2, which were fabricated simultaneously, showed only a slight difference in τ. Contact quality was determined mostly during the e-beam deposition process, which not only affects the normal-state transmission but also makes a drastic change in I_c and its T dependence, as predicted by the TI model.

In conclusion, the observed large I_cR_N product in our pGJJs in comparison with Δ_0/e points to SB Josephson coupling. The temperature dependence of I_c of the pGJJs deviated considerably from the conventional KO model. We demonstrate that $I_c(T)$ was well fit by the TI model, which correctly takes into account the effect of carrier transmission via the inhomogeneously doped graphene layer. We found that the detailed $I_c(T)$ is sensitive to the effect of carrier doping, which is represented by the parameter U/μ in the TI model. The shape of $I_c(T)$ near T_c is, however, mainly determined by the transparency of the graphene-superconductor contacts represented by the parameter r; e.g., $I_c(T)$ shows a convex downward dependence in the regime of a relatively small r, which is yet different from the conventional long-junction behavior. To summarize, we have identified the two crucial elements for characterizing a pGJJ: the effect of carrier

doping near the superconducting contacts and the quality of the graphene-superconductor interfaces. This key finding enables the correct characterization of SB strong Josephson coupling, which is essential for generating gate-tunable quantum states with high coherence.

*To whom all correspondence should be addressed.
hjlee@postech.ac.kr

[1] P. R. Wallace, Phys. Rev. 71, 622 (1947).

[2] K. S. Novoselov, A. K. Geim, S. V. Morozov, D. Jiang, M. I. Katsnelson, I. V. Grigorieva, S. V. Dubonos, and A. A. Firsov, Nature (London) 438, 197 (2005).

[3] Y. Zhang, Y.-W. Tan, H. L. Stormer, and P. Kim, Nature (London) 438, 201 (2005).

[4] D. K. Efetov, L. Wang, C. Handschin, K. B. Efetov, J. Shuang, R. Cava, T. Taniguchi, K. Watanabe, J. Hone, C. R. Dean, and P. Kim, Nat. Phys. 12, 328 (2016).

[5] Q. Zhang, D. Fu, B. Wang, R. Zhang, and D. Y. Xing, Phys. Rev. Lett. 101, 047005 (2008).

[6] C. W. J. Beenakker, Phys. Rev. Lett. 97, 067007 (2006).

[7] G.-H. Lee, D. Jeong, J.-H. Choi, Y.-J. Doh, and H.-J. Lee, Phys. Rev. Lett. 107, 146605 (2011).

[8] G.-H. Lee, D. Jeong, K.-S. Park, Y. Meir, M.-C. Cha, and H.-J. Lee, Sci. Rep. 5, 13466 (2015).

[9] H. B. Heersche, P. Jarillo-Herrero, J. B. Oostinga, L. M. K. Vandersypen, and A. F. Morpurgo, Nature (London) 446, 56 (2007).

[10] X. Du, I. Skachko, and E. Y. Andrei, Phys. Rev. B 77, 184507 (2008).

[11] D. Jeong, J.-H. Choi, G.-H. Lee, S. Jo, Y.-J. Doh, and H.-J. Lee, Phys. Rev. B 83, 094503 (2011).

[12] J.-H. Choi, G.-H. Lee, S. Park, D. Jeong, J.-O. Lee, H. S. Sim, Y.-J. Doh, and H.-J. Lee, Nat. Commun. 4, 2525 (2013).

[13] L. Bretheau, Ç. Ö. Girit, C. Urbina, D. Esteve, and H. Pothier, Phys. Rev. X 3, 041034 (2013).

[14] C. Janvier, L. Tosi, L. Bretheau, Ç. Ö. Girit, M. Stern, P. Bertet, P. Joyez, D. Vion, D. Esteve, M. F. Goffman, H. Pothier, and C. Urbina, Science 349, 1199 (2015).

[15] G.-H. Lee, S. Kim, S.-H. Jhi, and H.-J. Lee, Nat. Commun. 6, 6181 (2015).

[16] M. Kim, G.-H. Park, J. Lee, J. H. Lee, J. Park, H. Lee, G.-H. Lee, and H.-J. Lee, Nano Lett. 17, 6125 (2017).

[17] M. Ben Shalom, M. J. Zhu, V. I. Fal'ko, A. Mishchenko, A. V. Kretinin, K. S. Novoselov, C. R. Woods, K. Watanabe, T. Taniguchi, A. K. Geim, and J. R. Prance, Nat. Phys. 12, 318 (2016).

[18] I. V. Borzenets, F. Amet, C. T. Ke, A. W. Draelos, M. T. Wei, A. Seredinski, K. Watanabe, T. Taniguchi, Y. Bomze, M. Yamamoto, S. Tarucha, and G. Finkelstein, Phys. Rev. Lett. 117, 237002 (2016).

[19] V. E. Calado, S. Goswami, G. Nanda, M. Diez, A. R. Akhmerov, K. Watanabe, T. Taniguchi, T. M. Klapwijk, and L. M. K. Vandersypen, Nat. Nanotechnol. 10, 761 (2015).

[20] M. J. Zhu, A. V. Kretinin, M. D. Thompson, D. A. Bandurin, S. Hu, G. L. Yu, J. Birkbeck, A. Mishchenko, I. J. Vera-Marun, K. Watanabe, T. Taniguchi, M. Polini, J. R. Prance, K. S. Novoselov, A. K. Geim, and M. Ben Shalom, Nat. Commun. 8, 14552 (2017).

[21] G. Nanda, J. L. Aguilera-Servin, P. Rakyta, A. Kormányos, R. Kleiner, D. Koelle, K. Watanabe, T. Taniguchi, L. M. K. Vandersypen, and S. Goswami, Nano Lett. 17, 3396 (2017).

[22] A. A. Golubov, M. Y. Kupriyanov, and E. Il'ichev, Rev. Mod. Phys. 76, 411 (2004).

[23] M. Titov and C. W. J. Beenakker, Phys. Rev. B 74, 041401 (2006).

[24] Y. Takane and K.-I. Imura, J. Phys. Soc. Jpn. 80, 043702 (2011).

[25] Y. Takane and K.-I. Imura, J. Phys. Soc. Jpn. 81, 094707 (2012).

[26] I. O. Kulik and A. N. Omel'yanchuk, JETP Lett. 21, 96 (1975).

[27] I. O. Kulik and A. N. Omel'yanchuk, Sov. J. Low Temp. Phys. 3, 459 (1977).

[28] C. W. J. Beenakker, Phys. Rev. Lett. 67, 3836 (1991).

[29] L. Wang, I. Meric, P. Y. Huang, Q. Gao, Y. Gao, H. Tran, T. Taniguchi, K. Watanabe, L. M. Campos, D. A. Muller, J. Guo, P. Kim, J. Hone, K. L. Shepard, and C. R. Dean, Science 342, 614 (2013).

[30] H. Courtois, M. Meschke, J. T. Peltonen, and J. P. Pekola, Phys. Rev. Lett. 101, 067002 (2008).

[31] J.-H. Choi, Y.-J. Doh, and H.-J. Lee, J. Korean Phys. Soc. 57, 149 (2010).

[32] J. H. Lee, G.-H. Lee, J. Park, J. Lee, S.-G. Nam, Y.-S. Shin, J. S. Kim, and H.-J. Lee, Nano Lett. 14, 5029 (2014).

[33] A. L. Gudkov, M. Y. Kupriyanov, and K. K. Likharev, JETP Lett. 94, 319 (1988).

[34] A. V. Galaktionov and A. D. Zaikin, Phys. Rev. B 65, 184507 (2002).

[35] M. K. Weilmeier, W. H. Rippard, and R. A. Buhrman, Phys. Rev. B 61, 7161 (2000).

[36] B.-K. Kim, H.-S. Kim, Y. Yang, X. Peng, D. Yu, and Y.-J. Doh, ACS Nano 11, 221 (2017).

[37] A. Chrestin and U. Merkt, Appl. Phys. Lett. 70, 3149 (1997).

[38] See Supplemental Material at http://link.aps.org/supplemental/10.1103/PhysRevLett.120.077701 for data sets from additional devices and complementary explanations on the temperature dependence of the Josephson current including detailed description on the theoretical model.